J Intell Robot Syst (2011) 61:135–156
DOI 10.1007/s10846-010-9485-9

Evaluation of Guidance Performance in Urban Terrains for Different UAV Types and Performance Criteria Using Spatial CTG Maps

Zhaodan Kong · Bernie Mettler

Received: 1 February 2010 / Accepted: 1 September 2010 / Published online: 27 October 2010

Abstract Unmanned aerial vehicles (UAVs) present in a wide range of scales, airframe types and possible systems configurations. Assessing how these different systems perform, therefore, should be an essential part of their design. This task, however, is particularly difficult due to the complex, dynamic interactions these vehicles are capable of, and the often complex operational conditions. In this paper we describe and apply an evaluation framework based on spatial cost-to-go (SCTG) maps. These maps describe the spatial distributions of optimal state and cost-to-go for a given geographical environment, and are computed using a finite-state approximation of the vehicle dynamics. The SCTG maps embed the interaction effects between vehicle dynamics and environment, and thus provide a rigorous basis for the evaluation of the airframe, various system and environment factors. The paper describes the results obtained applying this framework to a basic goal-directed guidance task taking place in an urban environment. Three small-scale UAV types are compared: a fixed-wing aircraft, a standard helicopter, and a quad-rotorcraft. Both minimum-time and minimum-energy performance criteria are analyzed to determine overall performance characteristics and highlight the basic features of the proposed framework.

Keywords UAV · Autonomous guidance · Spatial cost-to-go function · Trajectory optimization · Performance evaluation

Z. Kong · B. Mettler (✉)
Department of Aerospace Engineering and Mechanics,
University of Minnesota, Minneapolis, MN 55455, USA
e-mail: mettler@aem.umn.edu

Z. Kong
e-mail: kong@aem.umn.edu

1 Introduction

Performance evaluation is a fundamental issue in the development of guidance systems for unmanned aerial vehicles (UAVs). Through quantitative evaluation, it is possible to measure the effect of different factors, including vehicle configurations, environments, and guidance and control system components. In addition, quantitative frameworks can provide an unambiguous representation to verify results, thus helping to assess new applications and prevent duplication of efforts [1].

Up to now, most of the performance evaluation works in the field of unmanned vehicles have focused on gathering metrics [2–4]. Those metrics, though meaningful, are normally mission and vehicle dependent. So it is difficult to use them to compare the performance across different systems. From a system's acquisition perspective, it is important to be able to evaluate the performance of different competing platforms. Such a need is especially pressing nowadays due to the rapid development of a wide range of UAVs based on a variety of airframe configurations with different dynamic capabilities [5, 6]. Furthermore, the majority of existing evaluations are performed based on flight data. The conclusions obtained from these evaluations, therefore, do not provide a direct feedback during the design process. Ideally, a quantitative evaluation framework should allow studying the effect of changes in airframe configuration, system and mission parameters, etc., thus providing insights into ways to improve the overall UAV design with respect to goals associated with mission profiles.

Paper [7] describes a first effort in benchmarking guidance algorithms. The basic idea is computing baseline trajectories for simple terrains, represented by geometric primitives, as well as actual urban terrains, represented by high resolution hight maps. Near time- or energy-optimal trajectories are generated for these environments using nonlinear programming (for the simple environments) and dynamic programming (for the actual urban environments). These near-optimal trajectories are then used as performance baselines to evaluate different guidance systems. One advantage of this work is that the framework provides a comprehensive picture where different factors such as environment characteristics can be studied. The works described in the present paper is an extension of the method from [7]. Here the general method is used to study the effects imposed by airframes and performance criteria. Further, the concept of spatial CTG maps are used here to begin to explore additional phenomena that are relevant from a more global perspective on guidance behavior and performance.

Related research can also be found in the fields of human factors [8] and human-vehicle teams [9, 10]. These efforts mainly concentrate on the human-vehicle interfaces and are mostly concerned with human factor measures such as reaction time and error rate. The human factor's field can provide relevant foundations to the evaluation of autonomous systems, in particular, the notion of 'behavior' can be extended to the 'vehicle's behaviors'. In fact, there exist several examples where robot performance has been studied based on concepts normally used in human-related or other social science areas [11–13].

The purpose of this paper is to describe the application of the guidance performance evaluation framework described in [14] to different UAV types and comparing the outcomes for performance indexes. The framework is based on optimal control formulation and enables quantifying influences of several individual

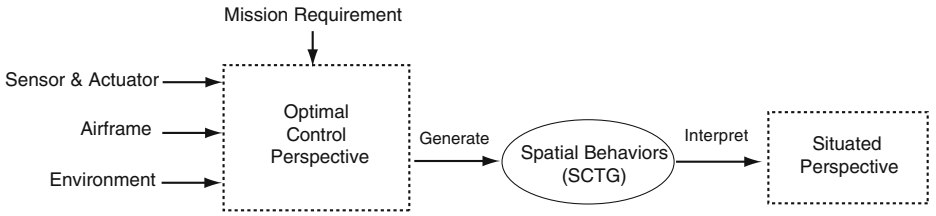

Fig. 1 Guidance performance evaluation framework. The guidance problem is formulated as an optimal control problem. Such a formulation provides a way to unify effects of different vehicle design, system components such as sensors and actuators, airframes, environments and mission requirements. Spatial behaviors generated based on this formulation are represented in the form of SCTG maps and trajectories. These maps and trajectories can then be analyzed providing a situated perspective necessary for a comprehensive evaluation of the system

factors on the overall performance. Factors of interests include dynamic capabilities, environment characteristics and mission requirements. The framework's key features are the following. First, it is based on an optimal control perspective [15, 16]. As shown in Fig. 1, optimal control principles are used to generate behaviors given a selected UAV system, environment, and a mission. This provides a basis to evaluate and compare performance across different vehicles and to investigate performance differences with respect to environment characteristics and choice of performance index. Second, the approach adopts a so-called situated perspective, which provides a way to study the guidance behavior as a function of environmental factors similar to the approach used in ecological psychology [12, 17].

The paper is organized as follows. The following section describes the optimal control formulation used as the foundation for the framework. In particular it introduces the concept of spatial cost-to-go (SCTG) map, which is an approximation of the optimal cost-to-go function and the associated optimal states. Section 3 first gives a brief overview of the three UAVs used in the paper (Hornet, MD4-200 UAV and Raven UAV), and then describes the approach used to build the motion primitive automaton (MPA) models based on the UAV type. The section also provides a short description of the algorithm used to compute the SCTG maps. Section 4 describes the results obtained applying the framework to a downtown section of San Diego. The results are presented from two different perspectives: first, for start-goal pairs, trajectories that are generated from the SCTG, and second, looking at characteristics of the entire SCTG maps. The last sections provides conclusions and an outline of the ongoing and future work.

2 Guidance Performance Evaluation Framework

As illustrated in Fig. 1, guidance behavior results from the interaction of the entire UAV system with the environment and task elements. The UAV itself combines multiple, coupled components, including airframe, sensors and actuators. The nature of guidance process dictates that their study and evaluation must be multi-component, multi-platform and situated with respect to the environments within which these vehicles are operating. In this paper we are mainly focused on

comparing the effect of airframe type (fixed-wind, helicopter and quad-rotorcraft) and performance criteria on overall guidance performance.

This section describes the proposed evaluation framework. Autonomous guidance is first formalized as an optimal control problem, which serves as a principle for driving the interaction of the UAV system and the operational environment. Instead of generating individual trajectories, a spatial cost-to-go (SCTG) map [14, 16, 18] is used to describe the vehicle's autonomous guidance behavior. These maps, which provide a spatial description of performance can then be analyzed to obtain insights into phenomena that would otherwise be difficult to identify by studying individual, point-to-point trajectories.

2.1 Autonomous Guidance as Optimal Control Problem

Classical aerospace guidance problems, such as orbit transfer of satellite or trajectory planning of long-range missiles, are usually solved as optimal control problems. The autonomous guidance of UAVs, especially those operating within cluttered environments, are much more challenging to solve as fully specified optimal control problems [16]. The reason for this is that guidance problems formulated as trajectory optimization problems are intrinsically NP-hard [19], which means that the computational complexity grows exponentially with the order of the vehicle's dynamics and the size of the environment. Since performance evaluation can be done offline, computational efficiency is less of a concern when used for an evaluation framework.

Formulating guidance problems as optimization problems has a number of benefits. First, it provides a way to account for the performance of each system components and the performance of the whole system within its operational environment. Such a formulation, thus, allows to analyze the relative contributions of the different components. Second, the optimization will drive the system performance and hence provides an opportunity to understand how vehicle flight-dynamic capabilities play out in the overall behavior. For instance, as we will show later, once a mission and its typical operational environment is given, such a formulation makes it possible to generate optimal behaviors for different UAVs thus providing a quantitative basis to compare their performance. Third, the optimal control framework provides a formal computational architecture and also a mathematical language to generate and describe operationally meaningful guidance behaviors. Although UAVs may not always operate according to their theoretical 'best' performances, it is a fact true that they cannot exceed the time-optimal performance. Thus a framework based on optimal control, allows setting a clear and objective upper bound on what is possible and then allows investigating how these 'best' performances are affected by different factors. Finally, an optimal control formulation provides the necessary foundations for future extensions to the framework. In particular to account for stochastic factors such as environment uncertainty or disturbances. Such a statistical approach would ultimately provide a way to capture real world conditions.

A general trajectory optimization formulation of a guidance task is to determine a control history $u(t)$ which will drive the vehicle from its current state x_0 to a desired goal state x_{goal} while minimizing a chosen performance objective of the form:

$$J_\infty(\mathbf{u}) = \int_{t_0}^{\infty} g(\mathbf{x}, \mathbf{u}) dt, \tag{1}$$

where g is the instantaneous cost function [16]. And the optimal command history $\mathbf{u}^*(t)$ at the current state $\mathbf{x}$ is given by:

$$\mathbf{u}^*_\infty(t) = \text{argmin}\{J^*_\infty(\mathbf{x})\}. \tag{2}$$

2.2 Framework for Situated Analysis

Guidance involves constant interactions between a vehicle and its environment, both via sensors and actuators. From a cognitive standpoint, the guidance performance depends on how an agent is able to use the 'affordances' associated with these interactions. Affordances are the perceived properties of an environment that are used by an agent to determine its behavior [12, 17, 20]. A particular urban environment will result in different 'affordances' for small UAVs (such as those investigated in this paper) than for a large ones (such as the Global Hawk). Affordances, therefore, depend not only on vehicles flight dynamics, but also on how these dynamic capabilities play out and can be utilized in a particular environment. To understand these phenomena, it is therefore necessary to study guidance as a spatial behavior. The idea of the framework is to describe the behavior as spatial distributions, i.e., vector fields, so as to be able to analyze the spatial characteristics of that guidance performance and identify phenomena that are associated with these critical aspects of these interactions.

2.3 Spatial Cost-to-go (SCTG) Framework

The optimal value function V^* and its associated optimal state $\mathbf{x}^*$ can be used to study such spatial characteristics and therefore provides a basis for an ecological approach to autonomous guidance. In [21], we showed that for Dubins' vehicle optimal guidance solution, in this case based solely on control considerations, gives rise to distinct spatial partitions. This structure, which is embedded in the optimal value function, significantly simplifies the control problem. Namely, the controls are the same for any starting points within a same partition, resulting in clusters of 'equivalent' trajectories. Therefore the vector field of each partition can be represented by a single quantity, providing a many-to-one mapping without loss of information. Hence, the complexity of the guidance problem is significantly reduced without a loss of performance. Such insights are important when studying complex guidance problems since they point to low-dimensional features in the coupled vehicle/environment system that can explain the system's behavior and performance.

The concept of SCTG function is first explicitly proposed in [16] as part of the receding horizon guidance framework. In the present paper, we use it as an analytical tool for studying guidance performance [14, 21]. The SCTG function is computed as an approximation of the problem's value function and its associated states based on a finite-state approximation of the vehicle dynamics and a discretization of the geographical environment. Such a formulation still enables to account for state-dependent performance indexes such as energy [14]. The details regarding the MPA model and SCTG computation are provided in the following Section 3.

Determining the value functions V^* involves solving the Hamilton-Bellman-Jacobi (HBJ) differential equation [22].

$$\frac{dV^*}{dt}(x,t) = -\left\{\frac{\partial V^*}{\partial x} f(\mathbf{x},\mathbf{u}) + g(\mathbf{x},\mathbf{u})\right\} \tag{3}$$

For most problems of practical interest, however, the HBJ equation cannot be solved analytically, therefore approximate, computational techniques have to be used to compute the value function. We call these approximate value functions together with their approximate solutions spatial cost-to-go (SCTG) functions [16]:

$$\Upsilon : x_f \mapsto \{V_S(x_f), v_S(x_f)\} \tag{4}$$

where $x_f \in F$ are the vector coordinates of a point in the geographical free space F. The corresponding optimal functional with respect to SCTG is:

$$\Upsilon^* : x_f \mapsto \{V_S^*(x_f), v_S^*(x_f)\} \tag{5}$$

where V_S^* is the optimal value function and v_S^* is the optimal velocity (see [16] for more details).

3 MPA Model & SCTG Computation

The motion primitive automaton (MPA) representation has originally been proposed as part of a hybrid guidance architecture [23, 24]. The benefit of the motion primitive formulation is the reduction in the complexity of the control problem. The optimization problem becomes a sequential decision problem, which can be solved as a dynamic programming problem.

In this section, we first provide a brief introduction of the UAVs used in the investigation and the procedure used to determine their respective MPA models. Subsequently, we provide a short description of the terrain data and the SCTG algorithm.

3.1 Overview of UAV Airframes

There are a variety of UAVs that are capable of performing surveillance and reconnaissance missions within urban terrain. In this paper, we choose three representative platforms: the Raven UAV from AeroVironment (http://www.avinc.com/), the Hornet UAV from Adaptive Flight (http://www.adaptiveflight.com/) and the MD4-200 UAV from Microdrones GmbH (http://www.microdrones.com/). Figure 2 shows their respective pictures along with their corresponding power curves. Table 1 summarizes the key physical and performance data based on public domain information. These three UAVs are based on different airframe configurations and hence are expected to have different dynamic capabilities. For instance, the Hornet UAV and MD4-200 UAV are capable of hovering. Stationary flight is critical for 'stare' type missions. The three UAVs also exhibit quite different power characteristics as shown in Fig. 2. These curves are computed from fixed and rotary wing flight mechanic

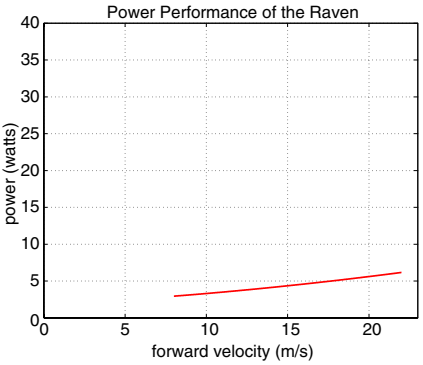

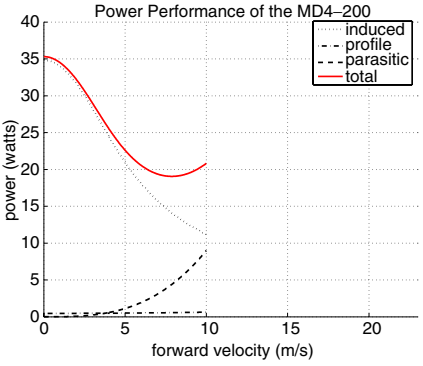

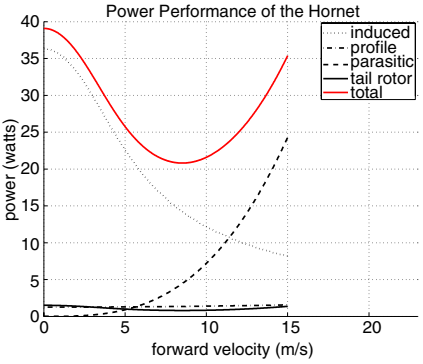

Fig. 2 UAVs investigated in this paper and their steady-state, level-flight power curves with respect to forward velocity. From *top to bottom*: the Raven from AeroVironment (http://www.avinc.com/), the Hornet UAV from Adaptive Flight (http://www.adaptiveflight.com/) and the MD4-200 UAV from Microdrones GmbH (http://www.microdrones.com/) (pictures taken from gopaultech.com, microdrones.com and adaptiveflight.com, respectively). The power curves convey the significant differences in their flight-performance characteristics

principles described in [25, 26] based on the parameters in Table 1. Power curves for the Hornet and MD4-200 UAV show the typical profiles common to rotorcraft. The total power comes from two parts: induced power and parasitic power. The first being the byproduct power of lift and the second being the power required

Table 1 Specification

	Hornet UAS[a]	Raven UAV[b]	MD4-200[c]
Weight (kg)	1.10	1.90	1.1
Length (m)	0.63	0.90	0.91
Width (m)	N/A	1.40	0.91
Height (m)	0.24	N/A	0.20
Rotor diameter (m)	0.71	–	0.37
Operating altitude (m)	1–150	30–152	<150
Duration (min)	20	60 to 90	20
Min speed (m/s)	0.00	8.89	0.00
Max cruise speed (m/s)	15.27	22.50	N/A
Max climb speed (m/s)	N/A	N/A	N/A

[a]from www.adaptiveflight.com
[b]from www.avinc.com
[c]from www.microdrones.com

to overcome the pressure and friction drags of the aircraft. While induced power decreases with increasing airspeed, parasitic power increases. For rotorcraft, the minimum power is usually achieved at a non-zero velocity. In another word, if we do not take power for vertical motion and acceleration into consideration, the most efficient flight configuration for the Hornet UAV or MD4-200 UAV is level and steady flight at their corresponding optimal airspeeds. The power curve for Raven UAV is more straightforward. It increases monotonously with respect to airspeed. Notice that Fig. 2 does not include descending or climbing power and acceleration is set to zero. During our MPA construction, however, these two additional factors will be considered (see [14] for more details).

The three chosen UAVs also share some similarities. For instance, as shown in Table 1, they have similar weights and dimensions. They also have similar operating altitudes and endurance. Their light-weight construction and small sizes make them suitable for easy deployment and thus are ideal for missions that require high-mobility.

3.2 Grid-Based Flight Envelope Motion Primitive Automaton

This section provides a brief description on how to construct a MPA model based on an example vehicle (see [14] for more details). A grid-based, finite-state MPA is a particular form of quantization of the vehicle dynamics where we constrain the motion primitives to share a common spatial grid [14, 27]. Using motion primitives defined on a fixed spatial grid prevents from having to perform costly interpolations during the value iteration. Furthermore, by using a heading resolution of $\pi/4$ allows to take advantage of symmetry in the rotation. Any motion primitive must be a combination of one horizontal motion primitive and one vertical motion primitive. A cost attribute can be assigned to each motion primitive. These can be based on various performance indexes can be used. Typical indexes that are operationally relevant include time or energy. Tactical criteria like visibility to a threat could also be used [28]. Of course, not any two horizontal and vertical motion primitives can be combined randomly. Their combination is restricted by the flight dynamics. For instance, for the Raven, the maximum vertical velocity is a function of the horizontal

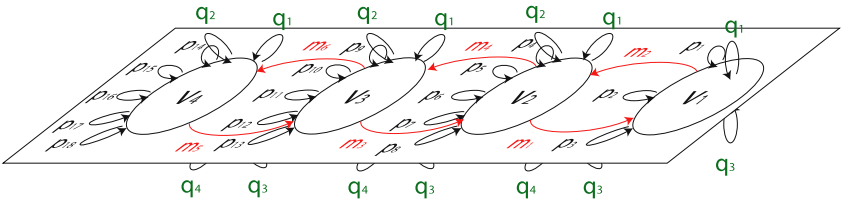

Fig. 3 An example MPA model. If there is a arrow from state a to state b, let's say from v_1 to v_2, it means that the UAV can make the transition from state a to state b. For this specified case it means that it can accelerate from v_1 to v_2

velocity, therefore. An example of MPA model, after these considerations have been accounted for, is shown in Fig. 3. In paper [7], solutions with MPA model were validated against those with nonlinear programming for some simple terrains. The latter solutions could be considered as the optimal ones. It was shown that the relative differences between the MPA solutions and the optimal solutions are within acceptable range, normally lower than six percent.

3.3 Digital Terrain Set

The terrain set used in this paper is a 2.44 m resolution Digital Terrain Elevation Data (DTED) map covering a 0.6 km by 1.2 km section of central San Diego. The section is depicted in Fig. 4. The data was generated from a low altitude aircraft LIDAR scan (available from the USGS website (http://lidar.cr.usgs.gov/)). The height map was extracted from the laser data by dividing the area covered by the data into square pixels and taking the maximum altitude sensed in each pixel. A very small number of outliers (fewer than 5) were removed by hand and replaced with 0 s.

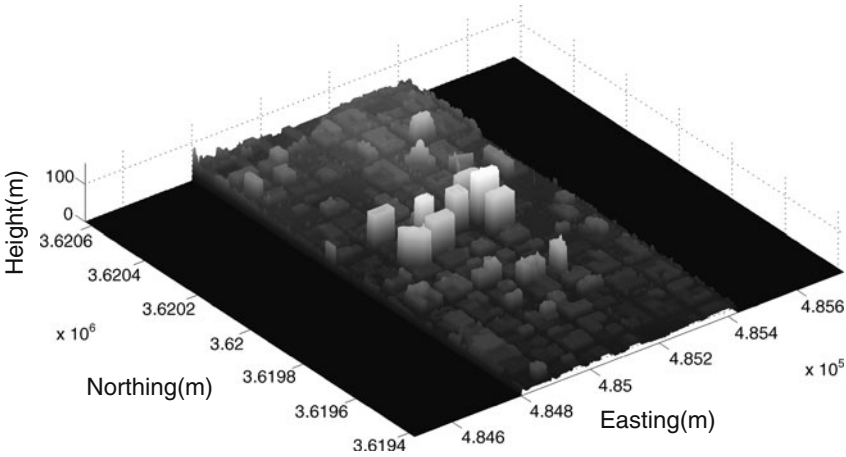

Fig. 4 DTED map used in this paper

3.4 SCTG Computation Algorithm

This section provides a brief overview of the algorithm used to compute the SCTG function (see paper [14] for details). For a given elevation map, goal state and motion primitive automaton, the algorithm computes the cost-to-go value, velocities and parent cell at each cell in the map. The algorithm is based on Dijkstra shortest path algorithm. It uses a Fibonacci heap data structure for efficient retrieval and update of the cells (nodes) [29].

Suppose the entire terrain volume is represented as a graph and each free node is represented as $x_f \in F \subset \mathbb{R}^3$. Three sets of data can be obtained after the SCTG calculation: the first one $V_S(F)$ records optimal CTG value $V_S(x_f) \in \mathbb{R}$ at each node x_f; the second one $v_S(F)$ records optimal velocity $v_S(x_f) \in \mathbb{R}^3$ at each node x_f and finally the third one $P_S(F)$ records parent node $P_S(x_f) \in \mathbb{R}^3$ of each node x_f. Notice that $V_S(F)$ is the traditional CTG function and the combination of $V_S(F)$ and $v_S(F)$ is what we call the SCTG map.

We formulate this problem into a graph search problem. Once the cells are initialized and the Fibonacci heap is constructed, in a loop, we fetch the unmarked cell v with minimum CTG, label the cell v, explore its neighbors and update their CTGs. Neighbors of the v are cells from which the helicopter can reach v with one of the given motions specified by the MPA. So each cell can have at most m neighbors, where m is the size of the motion primitive set used in the MPA. The number of edges in the graph is at most mn. The complexity of the algorithm for SCTG computation corresponds to that of the Dijkstra's shortest path algorithm with Fibonacci heap on a graph of n vertices and mn edges is $O(mn + nln(n))$ (assuming edge weights are non-negative)[29].

4 Results

This section describes the results obtained by applying the SCTG performance evaluation framework to the three UAV types. Two perspectives are provided. First, given any initial position, an optimal trajectory can be constructed from $P_S(F)$ along with the time histories of some of its key state variables, as well as their respective performance scores based on the performance criteria chosen in the SCTG computation. Second, the maps $v_S(F)$ and $V_S(F)$, in and of themselves, describe global characteristics of the interaction between the vehicle and the environment. Studying features found in the SCTG map can provide additional insights into relevant aspects of guidance performance. Combined these two perspective enable fundamental insights into aircraft design and guidance criteria on overall mission behavior.

4.1 Analysis Based on Optimal Trajectories

4.1.1 Generating Optimal Trajectories from the SCTG

The set $P_S(F)$ is stored in a tree data structure. The root of this tree is the goal and each branch represents a parent-child relationship between two nodes. In other words, if $P_S(x)$ is considered as a map $P_S(x_f) : \mathbb{R}^3 \mapsto \mathbb{R}^3$ that takes a node to its

parent node, for any node x_0 in the free space, a route can be constructed by applying map P_S iteratively as $P_S^m(x_0)$ until it reaches the goal.

The optimal trajectories can behave quite differently depending on the performance index used in the computation. These differences can be appreciated by inspecting their trajectories, associated trajectory characteristics and performances as measured by some chosen criteria. Figures 5, 6 and 7 show the optimal trajectories for the three UAVs for the time and energy performance indexes. The figures also show the time histories of state variables and their corresponding histograms for one of the starting points. Their time and energy performance scores are given in Tables 2 and 3. In these two tables, different rows correspond to different starting point and different columns correspond to different vehicle and different performance indexes. Take Table 2 (which is based on the minimum-time trajectories) for example, if we want to find the MD4-200 performance score from point A4, we first go to the columns for the MD4-200, and then go to the column for time, and finally go to the row for A4, which is 23.4 s. These results provide the basis to investigate the influences of aircraft types and performance indexes on guidance performance.

4.1.2 Influence of Aircraft Type on Trajectory

While all three UAVs can reach the goal from the six starting locations, their trajectories can be very different depending on whether time or energy is minimized. These difference illustrate how the flight-dynamic capabilities and energy profiles play out in the urban terrain environment.

The minimum-time trajectories of the Hornet and the MD4-200 have similar trajectories characteristics. They both stay 10 m away from the nearest building 40% of the time (as shown in their distance histograms). Note that 10 m is the safety distance that was specified and acts as a hard constraint for the minimum distance between aircraft and buildings. So in another word, the Hornet and the MD4-200 stay as close to the buildings as possible to achieve minimum-time performance. A typical trajectory is the one achieved by the MD4-200 from point A1: it essentially follows the streets, which are surrounded by tall buildings on both sides. As for the Raven, due to its inability to perform sharp turns that would allow it to fly around buildings, its minimum-time trajectories stay further away from the buildings. A typical trajectory for this aircraft is the one from point A6: it can be divided into three phases—a right turn phase to steer around buildings, a coast flight phase and finally a left turn phase with minimum turning radius to reach the goal. The minimum-energy trajectories behave quite similarly in the vertical direction for all three UAVs: they first climb until they clear buildings, then coast at a certain height and finally they descend. For the Hornet and the MD4-200, in the final descending phase, they still need power; while for the Raven, as shown from its power history in Fig. 7, in the last few seconds, there is no power expense. So in that final stage, it glides and uses the extra potential energy.

4.1.3 Influence of Performance Index on Trajectory

Individual differences can also be seen when inspecting their time and energy performance. For instance, for all the six starting points, as shown in Table 2, the Raven outperforms the Hornet, and the Hornet outperforms the MD4-200. The ranking happens to be consistent with their maximum velocities. However,

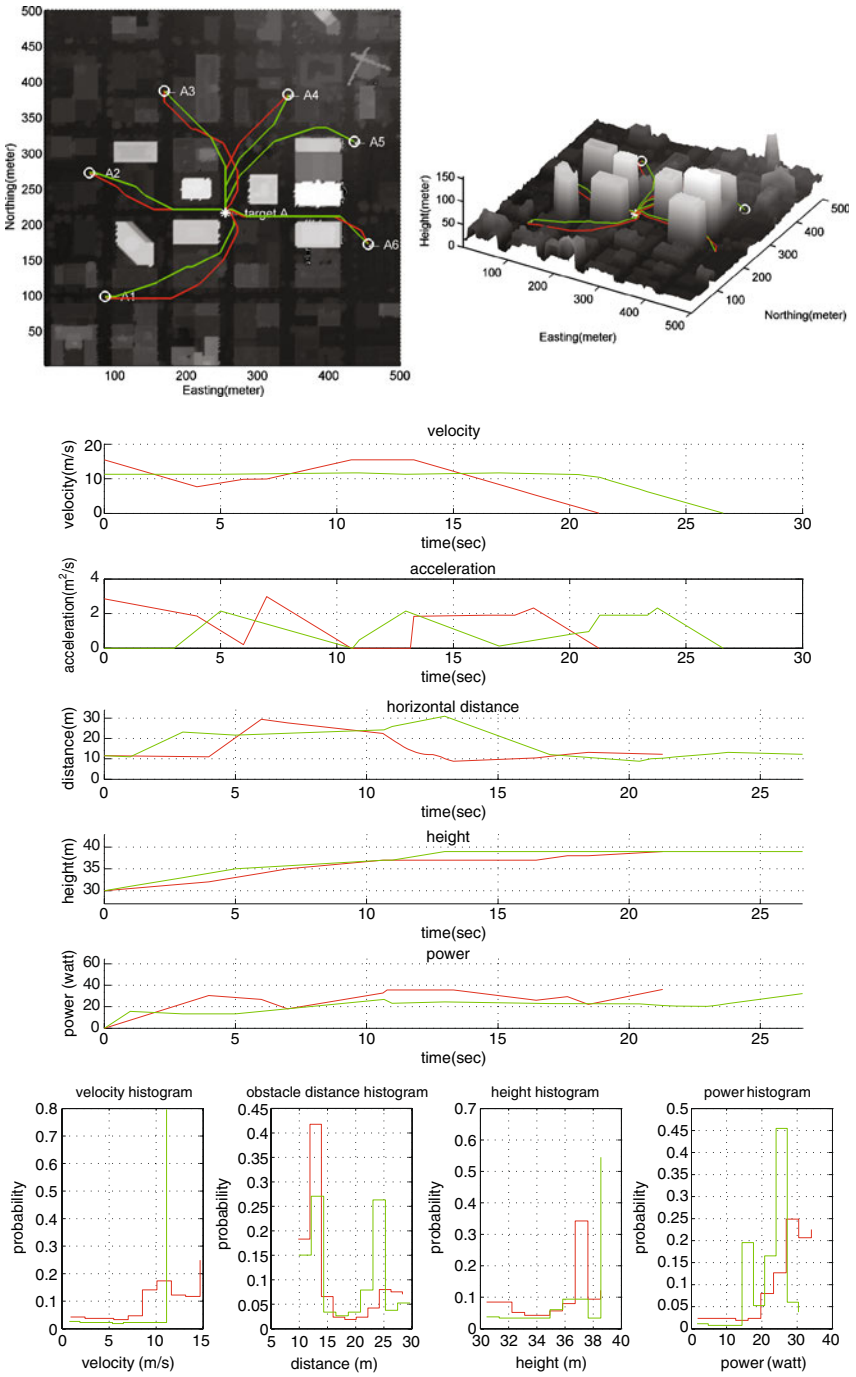
A1
A2
A3
A4
A5
A6
target A
Northing(meter)
Easting(meter)
Height(meter)
velocity
velocity(m/s)
time(sec)
acceleration
acceleration(m²/s)
horizontal distance
distance(m)
height
height(m)
power
power (watt)
velocity histogram
probability
velocity (m/s)
obstacle distance histogram
distance (m)
height histogram
height (m)
power histogram
power (watt)

◀ **Fig. 5** Optimal trajectories of the Hornet from six different points (A1 to A6). Time histories of a number of key variables (velocity, acceleration, distance to the nearest building, height and power, from *top to bottom*) and their histograms (velocity, distance to the nearest building, height and power, from *left to right*) for starting point A2 are shown on the *second* and *third row*. In this figure, Figs. 6 and 7, minimum-time trajectories, their corresponding time histories and histograms are illustrated as *red* and minimum-energy ones are illustrated as *green*

the relative performance differences achieved are quite smaller than the relative maximum velocity differences. For example, the mean time performance is 23.22 s for the Hornet and 27.52 s for the MD4-200, which corresponds to a difference of about 18%. The respective maximum velocities are 15.27 m/s and 10 m/s, corresponding to a relative maximum velocity difference of about 53%. The fact that maximum velocity does not translate entirely into a gain in performance highlights the importance of the interaction between dynamic capabilities and terrain. As shown from their velocity histories in Figs. 5 and 6, neither of them is able to fly at maximum velocity all the time.

We can also look at the effect the different performance indexes have on behavior. For all three UAVs, as can be expected, their minimum-time trajectories have a general tendency to follow high velocities. In contrast, their minimum-energy trajectories have a tendency to stay near a certain speed (11 m/s for the Hornet, 10 m/s for the MD4-200 and 18 m/s for the Raven). Notice that these speeds are different from their respective minimum-power speeds. To achieve minimum-energy, a UAV has to find the right tradeoff between power and flight duration. Take the Raven for example, while flying with its minimum-power speed (8.89 m/s) can save energy over a given flight duration, it also means that it has to spend more time to cover the same distance if it were flying at a higher speed. So after taking both of these factors into consideration, it settles to 18 m/s, which is neither the minimum-power speed nor the maximum flight speed.

Following the comparison based on UAV types, we can also gather interesting insights by comparing trajectories based on the performance indexes used to generate those. In Tables 2 and 3, values that are underlined correspond to the minimum values obtained when that particular performance index was used in the optimization. The other values provide an indication of the range of values that can be attained and the particular influence and specificity of a performance index. As seen from the last row of Table 2, the average time performances of minimum-energy trajectories for all the three UAVs are twice of those of minimum-time trajectories. The differences are not that dramatic for energy performance, as shown in the last row of Table 3.

4.2 Analysis Based on the SCTG Map

In contrast to point-to-point trajectories, the SCTG maps $(V_S(F), v_S(F))$, provide a global view and understanding of the way the dynamic capabilities, the goal condition, the environment and performance indexes interact and give rise to the spatial distribution describing the optimal vehicle behavior. For instance, the vector fields $v_S(F)$ for the MD4-200 and the Raven are illustrated in Fig. 9. In these figures, the vector at each free grid point x_f indicates the magnitude and direction of the

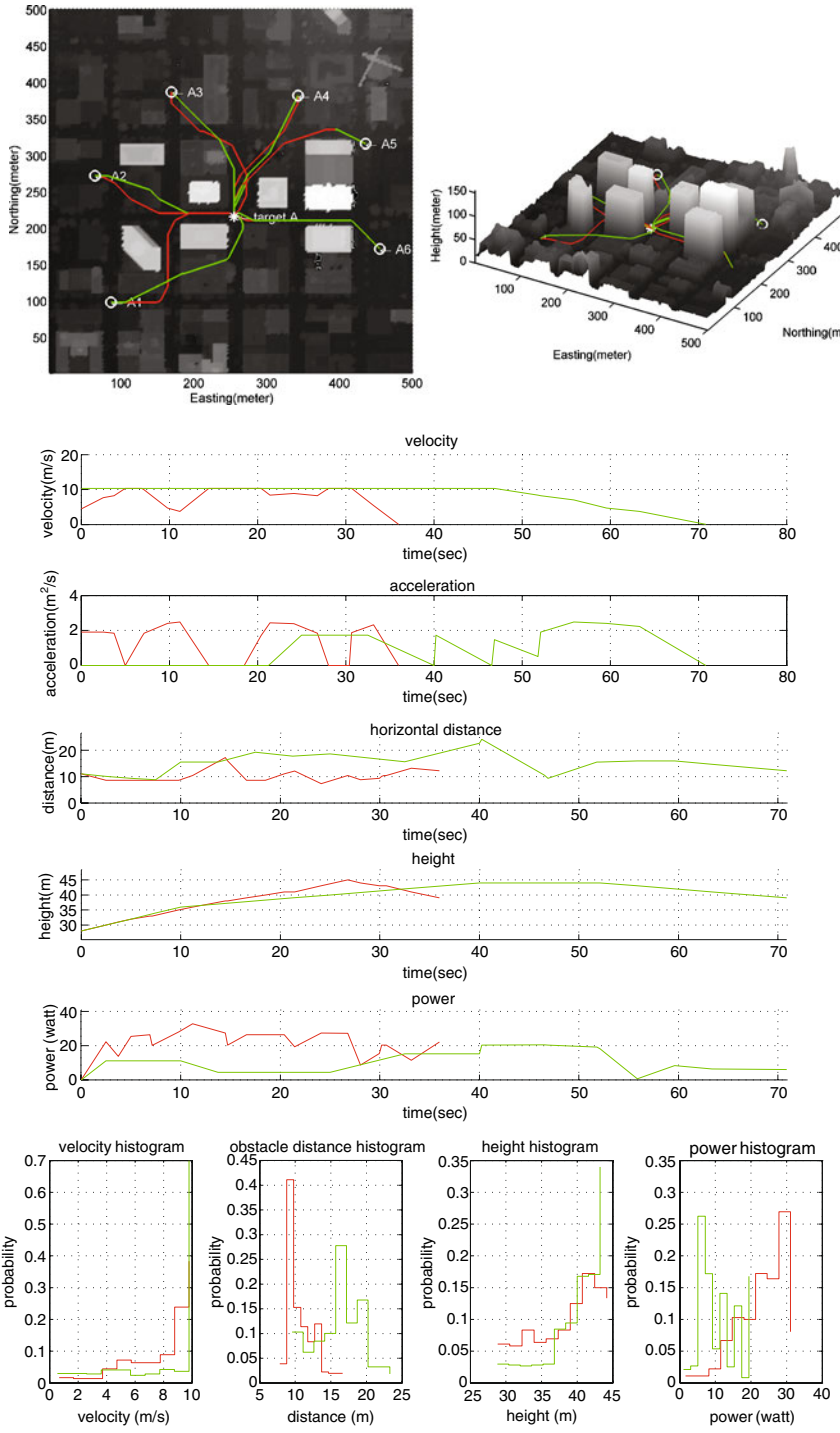

Fig. 6 Optimal trajectories and their statistical characteristics for the MD4-200

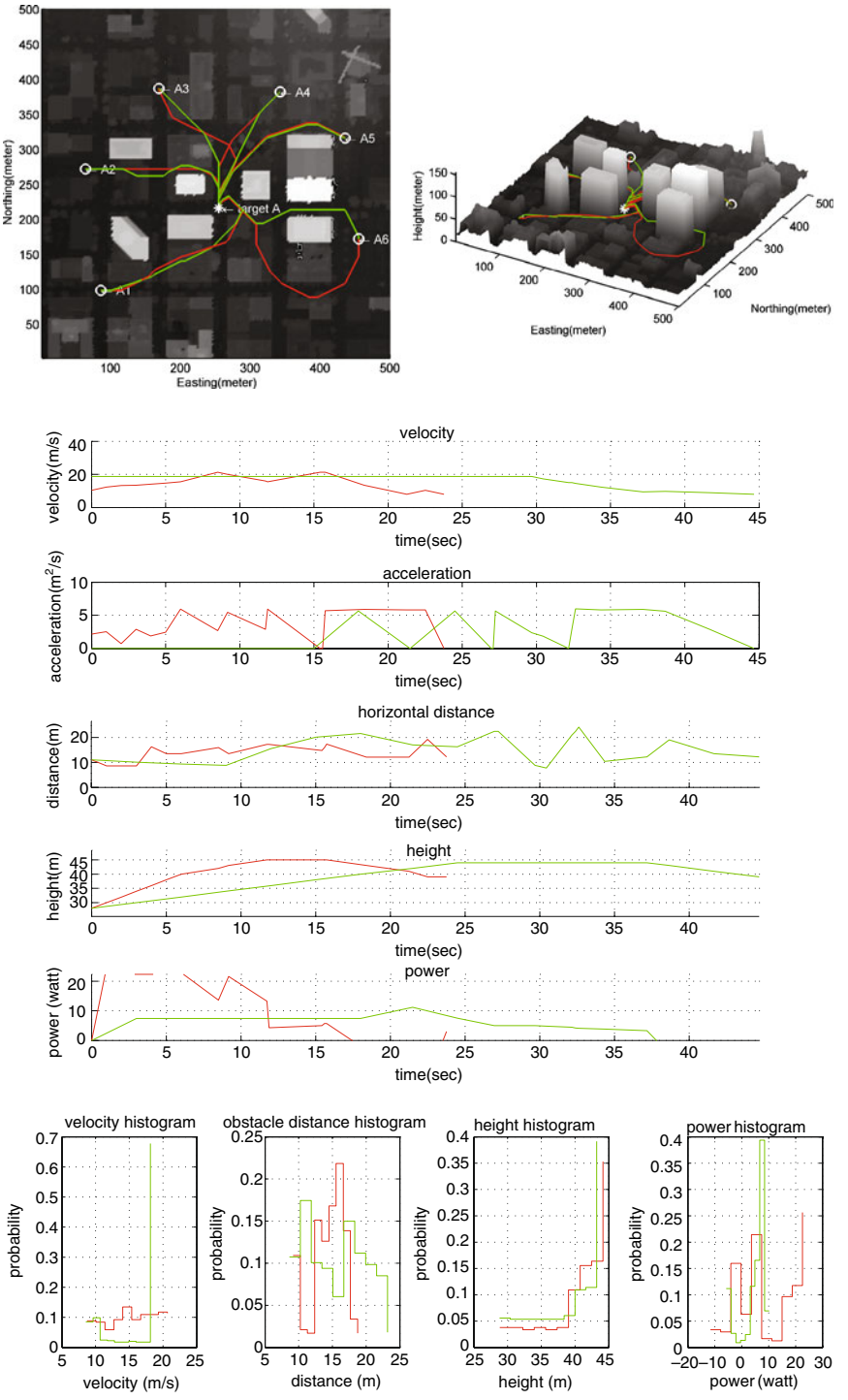

Fig. 7 Optimal trajectories and their statistical characteristics for the Raven

Table 2 Time performance of different vehicles obtained with different performance indexes (unit:second)

Vehicle	Hornet		MD4-200		Raven	
Performance index	Time	Energy	Time	Energy	Time	Energy
A1	31.38	47.33	35.99	70.86	23.76	44.68
A2	21.27	26.60	25.10	51.83	18.84	50.86
A3	23.48	93.01	26.65	96.39	16.36	53.66
A4	18.73	41.22	23.41	51.97	11.26	28.78
A5	22.35	43.33	27.90	49.45	14.76	26.31
A6	22.09	47.59	26.04	70.03	21.32	40.05
Mean	23.22	49.84	27.52	65.09	17.72	40.72
Relative difference (%)	114.68		174.65		129.87	

optimal velocity $v_S(x_f)$. Color is used to indicate the direction of vertical motion: yellow is used for level flight, red for descending and green for climbing flight respectively.

To illustrate the idea behind vector field map $v_S(F)$, suppose at each location in the free environment, there is a particle. As time evolves, these particles follow the velocity indicated by the vector field map as shown in Fig. 8. Such a process is analogous to the concept of pathline in fluid mechanics [30]. Vector field map provides a snapshot of the optimal behaviors, while figures such as the ones in Fig. 8 illustrate the full time history. Of course, here since the vector field is fixed, or steady in terms of fluid mechanics, the vector field in Fig. 9 and the particle locations in Fig. 8 convey equivalent information.

4.2.1 Characteristics of $V_S(F)$ and $v_S(F)$ Distributions

The map $v_S(F)$ helps to detect phenomena in a particular UAV behavior that may not be easily seen by investigating single trajectories. For example, for the area west of building 'A', the general minimum-time behavior for the MD4-200 is to move toward the street between building 'A' and building 'B'. For the Raven, on the other hand, the general behavior is to move to the northeast and steer around building 'A'. The reason for the different patterns is that considering that the final heading is to the south, while the MD4-200 can make a turn after it passes the street between 'A'

Table 3 Energy performance of different vehicles obtained with different performance indexes (unit:J)

Vehicle	Hornet		MD4-200		Raven	
Performance index	Time	Energy	Time	Energy	Time	Energy
A1	916.53	772.22	835.60	747.90	249.66	240.04
A2	645.97	610.39	610.80	598.09	322.26	270.06
A3	573.48	473.15	515.79	467.54	322.26	270.06
A4	359.78	328.59	326.45	316.16	111.20	110.86
A5	529.31	488.35	499.34	476.52	62.93	43.80
A6	658.79	632.34	618.31	598.34	196.81	193.08
Mean	613.98	550.84	567.72	534.09	188.67	160.15
Relative difference (%)	11.46		6.3		17.8	

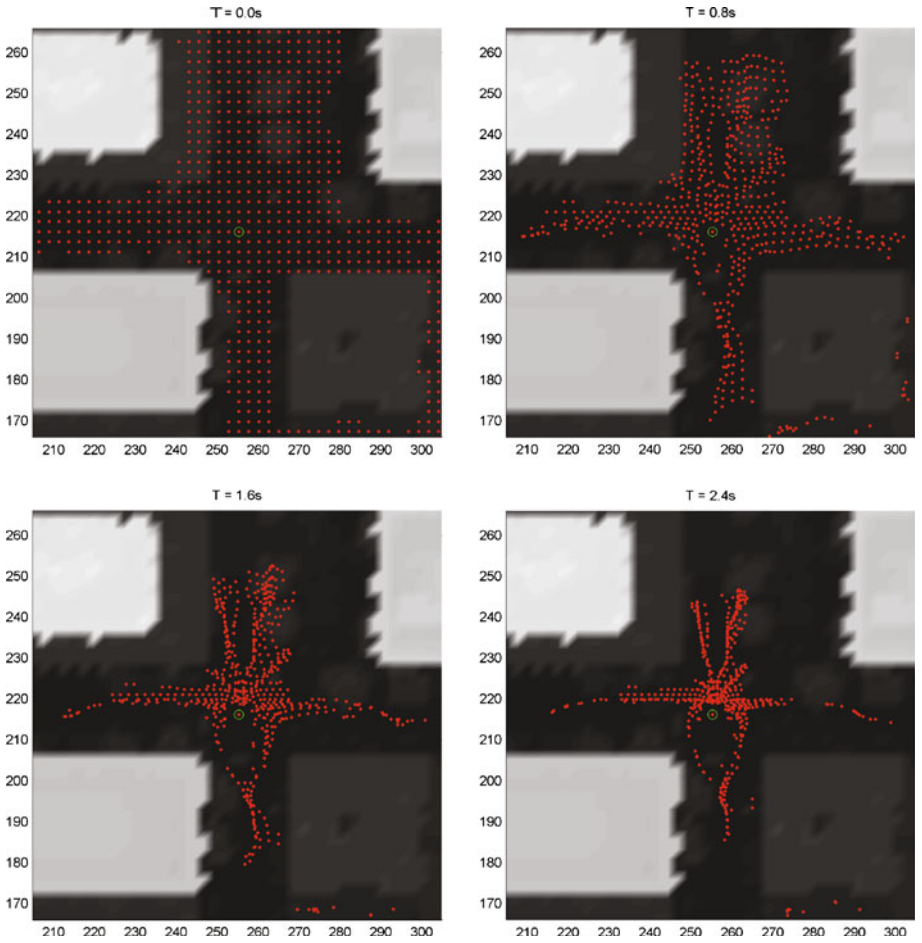

Fig. 8 Explanation of the vector field map $v_S(F)$. Suppose a particle is put at each free location as shown in the *upper-left* sub-figure. The locations of these particles at time 0.8, 1.6 and 2.4 s are illustrated in the other sub-figures. The case here corresponds to the MD4-200 with minimum time criterion. The corresponding vector field is in Fig. 9

and 'B', the Raven can not. This explanation is also valid for what happens at the southwest corner of building 'B' for the Raven. Instead of taking a more intuitive route, which is to fly around building 'B' clockwise, the Raven has to take a longer route, which is to fly clockwise with a larger circle and around building 'A'.

The map $v_S(F)$ can also help better understand the effect of different performance indexes. The difference between minimum-time and minimum-energy behavior for a same UAV, however, is not as dramatic as the difference seen between different UAVs with the same performance index, at least at the altitude shown in Fig. 9, which corresponds to the altitude of the goal. For many grid points x_f, the horizontal directions of velocity $v_S(x_f)$ for minimum-time and minimum-energy performance indexes are the same in this particular terrain. However, there exist many other locations where the horizontal directions are quite different, for instance, the southeast

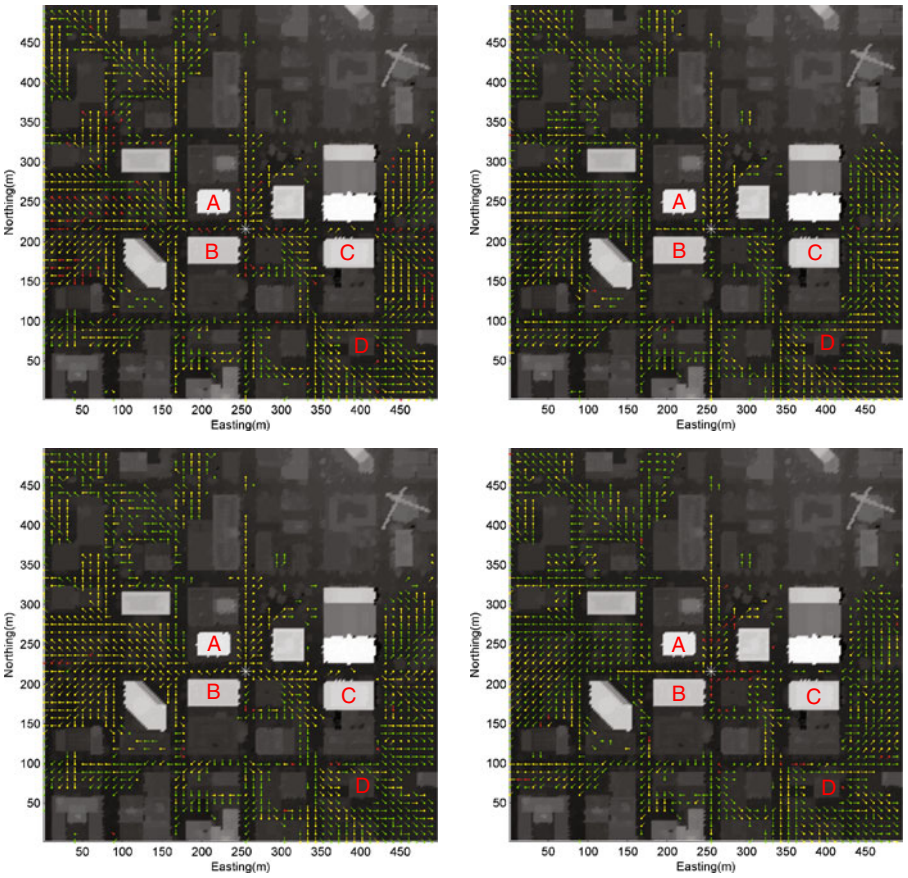

Fig. 9 Vector fields for different UAVs and different performance indexes. *First row* corresponds to the MD4-200 and *second row* corresponds to the Raven. *First column* corresponds to minimum-time performance index and *second column* corresponds to minimum-energy performance index. Since the behaviors of the Hornet and the MD4-200 are similar, only the vector fields of the MD4-200 are illustrated. In all these sub-figures, different colors mean different vertical velocity directions: *yellow* for level flight, *red* for descending and *green* for climbing. The goal is at the *center* of each figure and it is represented as a *white star*

corner of building 'C'. Moreover, vertical behavior can be quite different. For the minimum-energy behavior, the UAV tends to stay at the same height to save energy. This requires climbing first to reach an altitude that allows clearing buildings. The stored potential energy can then be used. While for minimum-time behavior, the UAV has more freedom to move up and downs. Such behavior is clearly shown in the upper-left sub-figure.

4.2.2 Embedded Structure in SCTG: the Virtual Arteries

The velocity distribution $v_S(F)$ is relatively uniform within certain areas, such as the west of building 'A'. In another word, trajectories starting from this area share a similar route. In contrast, in some areas, $v_S(x_p)$ can be different even for two

adjacent points. This is the case in the area at the southeast corner of building 'D'. In paper [21], we showed that such a phenomenon can be understood from a dynamical system standpoint [31]. For an optimal behavior in the plane, the free space embeds a partitioning structure defined by separatrices and sub-goals. For all the starting points within the same partition, their trajectories are 'equivalent' in the sense that they can be continuously deformed into each other without colliding with any obstacle. Furthermore, their control laws are the same, which is basically to move away from repelling manifolds and to approach the sub-goal corresponding to the partition that they belong to. After passing the first sub-goal, any trajectory starting from a same partition will follow the same 1D path. The collection of all these 1D paths forms a artery-like structure, with its root at the goal and the tips at the sub-goals. Here, we call such a structure 'virtual artery'. The virtual artery is embedded in the free space and reflects the salient structures within the guidance behavior, just as the role of the hierarchical generalized Voronoi graph (HGVG) in sensor-based exploration [32], only here the structure is a by-product of the interaction of the dynamics and the environment.

The concept of virtual artery can be extended to the 3D case. For instance, in Fig. 10, the minimum-time trajectories for a number of starting points behind building 'D' are plotted. Now based on the trajectories' behavior, the area behind the building can be divided into different partitions by 2D separatrices. And the following statements are still true: for all the starting points in a same partition, their optimal trajectories are equivalent and their local control laws are the same. The difference is that, for 3D cases, the trajectories leave a partition from a set of points

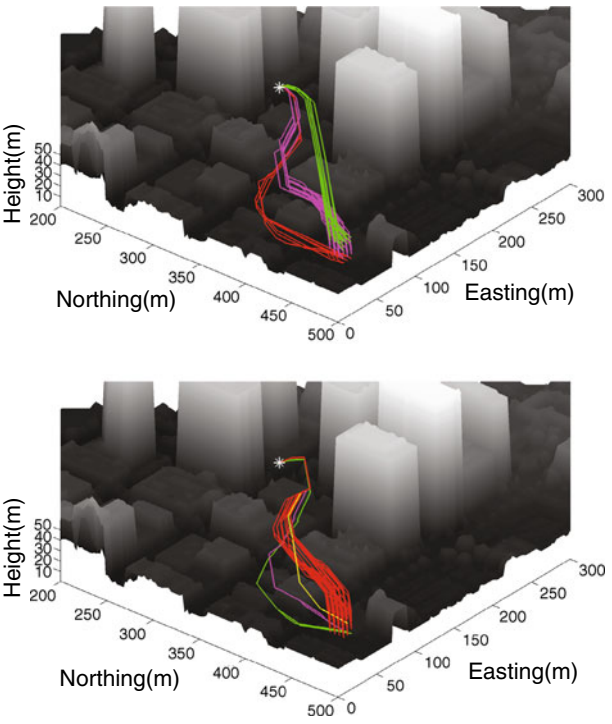

Fig. 10 'Virtual Artery' concept. These two figures illustrate the minimum-time trajectories from a number of points located at the southeast corner of building 'D'. The *upper* figure corresponds to the MD4-200 and the *lower* one corresponds to the Raven. Trajectories with the same color follow similar route. There are three different routes for MD4-200 and four for Raven. It is shown here that perturbation of the initial conditions will yield distinct families of trajectories. This is a typical characteristic of dynamical systems. These families can be viewed as virtual arteries of airways

instead of the single point in 2D cases and after they pass the point set, they follow a tube of paths instead of the single 1D path in 2D cases.

5 Conclusions and Future Work

Guidance performance results from the interplay of many factors, which include aspects related to flight-dynamic capabilities, UAV systems, guidance algorithm, performance criteria and environment. In this paper, we described an evaluation framework and applied it to different UAV types to illustrate the important effects aircraft type and performance indexes have on guidance behavior.

The proposed framework formulates guidance problem as an optimal control problem. To enable computation of solutions over an entire geographical environment, the vehicle dynamics are approximated using a motion primitive automaton (MPA). This formulation, makes it easy to compute the spatial distribution of optimal state and cost—the spatial cost-to-go (SCTG) maps—for any vehicle modeled as MPA, environment given as digital elevation map, and a pre-specified performance index.

Summary of Results The evaluation presented in the paper focused on three miniature UAV types: a fixed-wing aircraft, a standard helicopter and a quad-rotorcraft. Both time and energy performance criteria were investigated. SCTG map, computed for a section of the city of San Diego, provides a basis to analyze and compare the vehicle behavior. First, we compared individual differences in their trajectories and corresponding time histories for a number of starting locations in the environment. Second, we also analyzed the overall characteristics of their SCTG maps. The conclusions from these comparisons helps better understand the influences of UAV's dynamic capabilities and choice of performance criteria on UAV's overall guidance behavior. For instance, we were able to show that the Hornet and the MD4-200 share quite similar trajectory characteristics and overall spatial distribution of optimal behavior for the terrain investigated in this paper, while the Raven behaves quite differently.

Situated Perspective The SCTG maps offer a way to understand effects arising from the interaction between vehicle dynamics and its environment. How and to what degree a UAV can fulfill a guidance task depends on its embodiment, or what we could call dynamic 'fit', within its environment and how well it can take advantage of it to accomplish a task. For instance, the similarity in behaviors observed between the Hornet and the MD4-200, do not simply arise because they have similar airframe configurations—actually they have quite different ones—but their similar ability of attaining their functionality within a specific urban environment. If these two platforms were used in another type of environment, this interaction may play out differently, i.e., they would have a different dynamic fit. We would then expect to see different guidance behaviors and thus different functional abilities. This example illustrates that, when speaking of guidance performance, it is not sufficient to look at the vehicle alone; its operational environment and the dynamic interaction between the two also need to be taken into consideration. This type of analysis is known as 'situated perspective' and has received significant attention in the robotics community [12, 33].

Ongoing and Future Work The proposed framework is currently being extended to capture further system details. Particular attention is given to sensing, since it is an indispensable process for a UAV's guidance and the situated perspective provided by the framework should be very valuable. Being able to quantify the contribution of sensor in the interactions between environment and dynamics will lead to a more complete picture, in the sense of theory of affordance. We are also working on bringing uncertainty into the framework so as to better capture operational conditions as they exist in the real world. Being able to explicitly capture airframe and various systems components, and most importantly how these factors play out in a particular mission, will provide a valuable tool for the UAV design process. It should help understand where to put the focus of today's research and what type of sensing and flight-dynamic capabilities really translate into a gain in performance.

Acknowledgement This research work was enabled thanks to the financial support of NASA Ames (Grant Number NNX07AN31A).

References

1. Evans, J., Messina, E.: Performance metrics for intelligent systems. NIST Special Publication, pp. 101–104 (2001)
2. Sukhatme, G., Bekey, G.: Multicriteria evaluation of a planetary rover. In: Proceedings of IEEE International Conference on Robotics and Automation, pp. 22–28 (1996)
3. Wong, S., Middleton, L., MacDonald, B., Auckland, N.: Performance metrics for robot coverage tasks. In: Proceedings of Australasian Conference on Robotics and Automation, vol. 27, p. 29 (2002)
4. Tunstel, E.: Operational performance metrics for mars exploration rovers: field reports. J. Field. Robot. **24**(8–9), 651–670 (2007)
5. Pines, D., Bohorquez, F.: Challenges facing future micro-air-vehicle development. J. Aircr. **43**(2), 290–305 (2006)
6. Costello, M.: Challenges facing micro air vehicle flight dynamics and controls engineers. 46th AIAA Aerospace Sciences Meeting and Exhibit. Reno, NV (2008)
7. Mettler, B., Kong, Z., Goerzen, C., Whalley, M.: Benchmarking of obstacle field navigation algorithms for autonomous helicopters. American Helicopter Society 66th Annual Forum. Phoenix, AZ (2010)
8. Hollands, J., Wickens, C.: Engineering Psychology and Human Performance. Prentice Hall (1999)
9. Rodriguez, G., Weisbin, C.: A new method to evaluate human-robot system performance. Auton. Robots **14**(2), 165–178 (2003)
10. Cummings, M., Bruni, S., Mercier, S., Mitchell, P., et al.: Automation architecture for single operator, multiple UAV command and control. The International C2 Journal **1**(2), 1–24 (2007)
11. Smithers, T.: On quantitative performance measures of robot behaviour. Robot. Auton. Syst. **15**(1–2), 107–133 (1995)
12. Nehaniv, C., Dautenhahn, K.: Of hummingbirds and helicopters: an algebraic framework for interdisciplinary studies of imitation and its applications. In: Demiris, J., Birk, A. (eds.) World Scientific Series in Robotics and Intelligent Systems, Interdisciplinary Approaches to Robot Learning, vol. 24, pp. 136–161. World Scientific Press (2000)
13. Nehmzow, U.: Quantitative analysis of robot-environment interaction–towards scientific mobile robotics. Robot. Auton. Syst. **44**(1), 55–68 (2003)
14. Kong, Z., Korukanti, V., Mettler, B.: Mapping 3D guidance performance using approximate optimal cost-to-go function. AIAA Guidance Navigation and Control Conference. Chicago, IL (2009)
15. Bellman, R., Dreyfus, S.: Applied Dynamic Programming. Princeton University Press
16. Mettler, B., Dadkhah, N., Kong, Z.: Agile autonomous guidance using spatial value functions. Control Eng. Pract. **18**(7), 773–788 (2010)

17. Gibson, J.: The ecological approach to the visual perception of pictures. Leonardo **11**(3), 227–235 (1978)
18. Mettler, B., Toupet, O.: Receding horizon trajectory planning with an environment-based cost-to-go function. In: Proceedings of IEEE Conference on Decision and Control, pp. 4071–4076 (2005)
19. Reif, J.: Complexity of the mover's problem and generalizations extended abstract. In: Proceedings of the 20th Annual IEEE Conference on Foundations of Computer Science, pp. 421–427 (1979)
20. Hutchins, E., Lintern, G.: Cognition in the Wild. MIT, Cambridge (1996)
21. Kong, Z., Mettler, B.: On the general characteristics of 2d optimal obstacle-field guidance solution. IEEE Conference on Decision and Control. Shanghai, China (2009)
22. Bryson, A., Ho, Y.: Applied Optimal Control. Wiley, New York (1975)
23. Lynch, N., Segala, R., Vaandrager, F.: Hybrid I/O automata revisited. In: Domenica Di Benedetto, M., Sangiovanni-Vincentelli, A. (eds.) Hybrid Systems: Computation and Control. Lecture Notes in Computer Science, World Scientific Series in Robotics and Intelligent Systems, vol. 2034, pp. 403–417. Rome, Italy (2001)
24. Frazzoli, E., Dahleh, M., Feron, E.: Robust hybrid control for autonomous vehicle motion planning. In: Proceedings of IEEE Conference on Decision and Control, vol. 1 (2000)
25. Leishman, J.: Principles of Helicopter Aerodynamics. Cambridge Universtiy Prress (2006)
26. McCormick, B.: Aerodynamics, Aeronautics, and Flight Mechanics. Wiley (1995)
27. Mettler, B., Kong, Z.: Receding horizon trajectory optimization with a finite-state value function approximation. American Control Conference, pp. 3810–3816 (2008)
28. Mettler, B., Bachelder, E.: Combining on-and offline optimization techniques for efficient autonomous vehicles trajectory planning. AIAA Guidance, Navigation and Control Conference and Exhibit. San Francisco, CA (2005)
29. Fredman, M., Tarjan, R.: Fibonacci heaps and their uses in improved network optimization algorithms. Journal of the ACM (JACM) **34**(3), 596–615 (1987)
30. Fox, R., McDonald, A., Pritchard, P.: Introduction to Fluid Mechanics. Wiley, New York (1985)
31. Chicone, C.: Ordinary Differential Equations with Applications. Springer, Verlag (2006)
32. Choset, H., Burdick, J.: Sensor-based exploration: the hierarchical generalized voronoi graph. Int. J. Rob. Res. **19**(2), 96 (2000)
33. Zender, H., Jensfelt, P., Mozos, O., Kruijff, G., Burgard, W.: An integrated robotic system for spatial understanding and situated interaction in indoor environments. In: Proceedings of the National Conference on Artificial Intelligence, vol. 22, pp. 1584–1589 (2007)